An Improved Joint Detection of Integer Frequency Offset and Sector Cell Index for LTE Downlink

Rih-Lung Chung*, Jian-Wei Huang

***Abstract*—In this paper, we propose the joint integer frequency offset (IFO) and sector cell index (CID) for the LTE downlink system. First, we use the symmetry property of the phase difference samples of the primary synchronization signal (PSS) in the algorithm design, and thus the hardware complexity of proposed detection algorithm can be reduced. Second, we analyze the real part and the imaginary part of phase-difference correlation of the PSS, and find that only its real part values provide positive information to the algorithm. Therefore, we apply this critical result to the detection algorithm design further to improve the detection performance. Simulation results show that our proposed joint detection algorithm can not only reduce the requirements of multipliers up to 50%, but also can improve the detection performance for more than 4 dB. Moreover, in the case of not compensating small scale of fractional frequency offset (FFO), the detection performance can also achieve acceptable detection performance.**

***Index Terms*—Primary synchronization signal (PSS), integer frequency offset (IFO), synchronization, sector cell index.**

I. Introduction

THE long term evolution (LTE) is the advanced version of the 3GPP for fulfilling transmission targets of four generation (4G) mobile communication system. The downlink LTE system adopts orthogonal frequency division multiple access (OFDMA) technique both for combating the multipath effect of frequency selective channel and for achieving high data rates.

In the LTE system, synchronization plays an important role in the system performance. Generally speaking, the synchronization problems can be divided into timing and frequency synchronizations; the former mainly deals with estimating transmission propagation delay, and the latter mainly for estimating the mismatch frequency between the transmitter's and the receiver's oscillators. Thus, the user equipment (UE) of the LTE first needs to obtain some synchronization parameters for latter synchronization, such as symbol timing, frame time, carrier frequency offset (CFO), sector cell index (CID), and cell identity group, and etc. In this paper, we aim at dealing with the estimations of CFO and sector CID because they highly dominate the performance of the LTE system.

In general, the CFO problem can be divided into fractional frequency offset (FFO) and integer frequency offset (IFO) problems, and the designs of CFO estimation algorithms can be based on data-aided, non-data aided, or cyclic prefix (CP) [2-5]. In [2] and [5], the FFO algorithms are CP based, and thus system bandwidth can be saved for data transmission. The authors used the known pilots and applied the maximum likelihood (ML) rule to design IFO detection algorithm [3], [4]. As for estimating sector CID, the authors proposed a low complexity sector CID search procedure for the multipath channel [6]. However, this procedure requires channel response estimation, and the algorithm performance is highly sensitive to the degree of channel estimation accuracy. In [7], the joint detection algorithm of IFO and sector CID is therefore proposed for achieving better detection performance. However, the joint detection algorithm suffers from higher computing complexity.

In this paper, we use the symmetry property of phase-difference samples of the PSS of the LTE to reduce the computing complexity. Besides, we analyze the real part and the imaginary part of phase-difference correlation of the PSS, and find that only its real-part values provide positive information to the algorithm. Therefore, we apply this critical result to the detection algorithm design further to improve the detection performance. The remaining of the paper is organized as follows. In Section II, the LTE structure is described. In Section III, the system model of the downlink LTE system is constructed. In Section IV, several synchronization algorithms are briefly overviewed, and the joint synchronization detection algorithm with low complexity and high detection performance is proposed. Simulation results are conducted in Section V. Finally, concluding remarks are made in Section VI.

II. LTE Structure

The LTE transmission frame structures can be frequency division duplex (FDD) or time division duplex (TDD) [1]. In the both frame structures, one frame time is 10 ms, and consists of 10 sub-frames or 20 time slots. Thus, one sub-frame is 1 ms, and one time slot is 0.5 ms. In the LTE, there are normal CP (NCP) mode and extended CP (ECP) mode; the former has 7 OFDM symbols, and the latter has 6 OFDM symbols [1]. In this paper, we adopt NCP mode.

*Corresponding author: Rih-Lung Chung is with Department of Electronic Engineering, Chung Yuan Christian University, Chungli City, 32023, Taiwan. He is now an Assistant Professor in Department of Electronic Engineering. (e-mail: rlchung @cycu.edu.tw).

Jian-Wei Huang is with Chung Yuan Christian University, Chungli City, 32023, Taiwan, He is now with the Department of Electronic Engineering.(e-mail: g10076028 @cycu.edu.tw).

ISBN: 978-988-19252-6-8
ISSN: 2078-0958 (Print); ISSN: 2078-0966 (Online)

As for synchronization signals, the LTE defines primary synchronization signal (PSS), secondary synchronization signal (SSS), and reference signal (RS). In this paper, we use PSS for estimating synchronization parameters.

A. Primary Synchronization Signal (PSS)

The PSS is made of length-62 Zadoff-Chu (ZC) sequence, and inherits constant envelope and perfect auto- and cross correlations of the ZC sequence. Thus, the PSS is used as pilots for the LTE system. The frequency-domain ZC sequence associated with root index u is given by $d_u(n)$, for n=0, 1, …, 61.

$$d_u(n)=\begin{cases} e^{-j\frac{\pi un(n+1)}{63}} & n=0,1,\ldots,30 \\ e^{-j\frac{\pi u(n+1)(n+2)}{63}} & n=31,32,\ldots,61 \end{cases} \quad (1)$$

Besides, the value of u for different sector CID $N_{ID}^{(2)}$ is defined in TABLE I.

TABLE I.
Sector CID $N_{ID}^{(2)}$ and root index u

$N_{ID}^{(2)}$	**Root index *u***
0	25
1	29
2	34

B. PSS and SSS Frame Structures

The PSS and SSS are pilot signals of the LTE system for synchronization. In the LTE FDD mode [1], the PSS and the SSS are both placed on the time slot 0 and time slot 10, as shown in Fig. 1. Here, the same PSS sequence modulates 62 subcarriers of the sixth OFDM signal of both time slots. Different SSS sequences modulate 62 subcarriers of the fifth OFDM signal of both time slots.

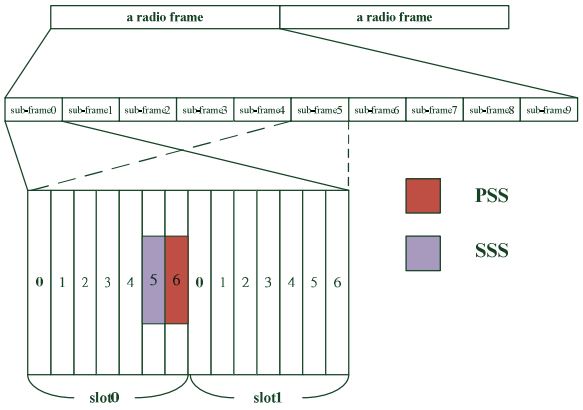

Fig. 1. Synchronization signals of the LTE system.

III. System Model of LTE Downlink

In this section, we construct the OFDMA system model. The time-domain OFDMA signal corrupted by the CFO is given by

$$r_{l,n}=\left(x_{l,n}\otimes h_{l,n}\right)\cdot e^{j2\pi\varepsilon_{CFO}(n+l(N+G))/_{FFT}}+w_{l,n} \quad (2)$$

where $r_{l,n}$ is received signal at the nth sample of the lth OFDMA symbol. Here, channel response is $h_{l,n}$, and transmitted signal is $x_{l,n}$, for l is the OFDMA symbol index, and $n\in[1, N+G]$ is the sample index; N is the FFT length, G is the CP length, and $w_{l,n}$ is an additive white Gaussian noise; ε_{CFO} is the CFO, and $\otimes$ denotes convolution. After removing the CP of $r_{l,n}$ and taking FFT on the $r_{l,n}$, we may obtain frequency-domain signal $R_{l,k}$.

$$R_{l,k}=\alpha\cdot X_{l,k-\varepsilon_{IFO}}\cdot H_{l,k-\varepsilon_{IFO}}+\beta_{l,k-\varepsilon_{IFO}}+W_{l,k-\varepsilon_{IFO}} \quad (3)$$

where

$$\alpha=\frac{\sin(\pi\varepsilon_{FFO})}{N\sin(\frac{\pi\varepsilon_{FFO}}{N})}\cdot e^{j2\pi\frac{l(N+G)+G}{N}(\varepsilon_{CFO})}\cdot e^{j\pi\frac{N-1}{N}(\varepsilon_{FFO})} \quad (4)$$

and

$$\beta_{l,k-\varepsilon_{IFO}}=\sum_{p=-N/2+1,\,p\neq k-\varepsilon_{IFO}}^{N/2}X_{l,p}\cdot H_{l,p}\cdot\frac{\sin(\pi(p+\varepsilon_{CFO}-k))}{N\cdot\sin(\frac{\pi(p+\varepsilon_{CFO}-k)}{N})}\cdot e^{j2\pi\frac{l(N+G)+G}{N}\cdot(\varepsilon_{CFO})}\cdot e^{j\pi\frac{N-1}{N}\cdot(p+\varepsilon_{CFO}-k)} \quad (5)$$

and

$$\varepsilon_{CFO}=\varepsilon_{FFO}+\varepsilon_{IFO} \quad (6)$$

where $R_{l,k}$ is the received signal on the lth symbol and kth subcarrier; $H_{l,k}$ is the (l,k)th channel frequency response, $X_{l,k}$ is the transmitted symbol, *and* $W_{l,k}$ is AWGN, for $k\in[-N/2, N/2]$. The CFO is divided into two parts, i.e., FFO ε_{FFO} and IFO ε_{IFO}.

IV. Synchronization Procedure

In this section, we first review the FFO and IFO estimation algorithms, which are described in Sec. IV.*A* and Sec. IV.*B*, respectively. Then, we propose an improved joint detection algorithm of IFO and sector CID in Sec. IV.*C*.

A. ML Estimation of the FFO

Supposed that the CP length is known, our first work is to detect the symbol boundary. After estimating the symbol boundary, the starting position of the FFT window can be correctly determined, and thus the FFT operation can be correctly performed. In this paper, we adopt the normalized method for detecting symbol boundary [5]. The detection algorithm is given below,

$$\hat{\phi}_{N,M}(m)=\left\{\frac{\left|\sum_{g=0}^{G-1}r_{l,m-g}\cdot r^{*}_{l,m-g-N}\right|}{\left|\sum_{g=0}^{G-1}r_{l,m-g}\cdot r^{*}_{l,m-g}\right|}\right\} \quad (7)$$

ISBN: 978-988-19252-6-8
ISSN: 2078-0958 (Print); ISSN: 2078-0966 (Online)

$$m_{boundary} = \arg\max_{m} \quad \hat{\phi}_{N.M}(m) \tag{8}$$

where $m_{boundary}$ is the starting position of the frame. Because the detection of FFO lies in using the correlation between the CP and OFDM symbol, we may use the similar method for estimating FFO, which is given below.

$$\hat{\varepsilon}_{FFO} = -\frac{1}{2\pi}\angle\left(\max_{m} \hat{\phi}_{N.M}(m)\right) \tag{9}$$

where G is the CP length, and l is the OFDMA symbol index. The estimated FFO $\hat{\varepsilon}_{FFO}$ is only in the range (-0.5, 0.5), and thus the excess CFO that is beyond the range of FFO will be compensated by the IFO correction.

B. Joint Detection of IFO and Sector CID

After compensating the effect of FFO, there still remains IFO effect. In the light of equation (3), we may know that the IFO causes the transmitted signal to be on the wrong subcarrier. To be specific, the transmitted signal is modulated on the $(k\text{-}\varepsilon_{IFO})$th subcarrier, but the associated received signal is changed to be on the kth subcarrier and thus causes the detection error. Besides the IFO, the sector CID is also important parameter for LTE synchronization. Thus, in this paper we consider the joint detection problem of IFO and sector CID by using the PSS information. Assuming that FFO and symbol timing are perfect compensation, the joint synchronization detection of IFO and sector CID is given below [7].

$$\begin{aligned} &C_1(i,u) \\ &= \sum_{k=-31}^{-2} \left\{R_{PSS}(k+1+i)\cdot R_{PSS}^{*}(k+i)\right\}\cdot\left\{d_u(k+32)\cdot d_u^{*}(k+31)\right\}^{*} \\ &+ \sum_{k=1}^{30} \left\{R_{PSS}(k+1+i)\cdot R_{PSS}^{*}(k+i)\right\}\cdot\left\{d_u(k+31)\cdot d_u^{*}(k+30)\right\}^{*} \end{aligned} \tag{10}$$

and

$$\left(\hat{\varepsilon}_{IFO}, \hat{u}\right) = \arg\max_{i,u} \left|C_1(i,u)\right| \tag{11}$$

where R_{pss} is the frequency domain received signal associated the PSS pilot index. From (11), we may know that the optimal shift index i and root index u can be obtained by maximizing the cost function (11), where the range of the IFO is in (-31, 31).

C. Improved Joint Detection of IFO and Sector CID

Because the PSS is made of the ZC sequence, we can first use the symmetry property of the sequence further to reduce the computing complexity of the detection algorithm (11). In so doing, up to 50% requirements of the multipliers can be saved. Fig. 2 shows the symmetry property of the PSS. It shows that the signal can be regarded as an even function, where the first 31 samples and the last 31 samples are even symmetry.

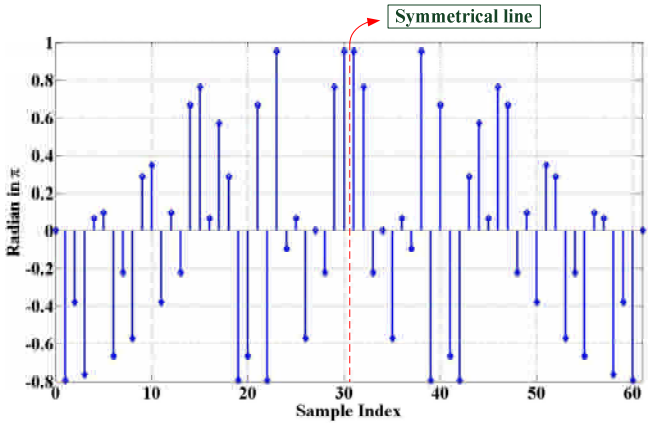

Fig. 2. Phase variation of the PSS (radian in π)

Note that in the equation (10) the first 30 phase-difference samples $d_u(k+32)\cdot d_u^{*}(k+31)$, for k =-31, -30, …, -2, and the last 30 phase-difference samples $d_u(k+31)\cdot d_u^{*}(k+30)$, for k=1, 2, …, 30, are odd symmetry. Therefore, by making good use of this symmetry property, the complexity of cost function (10) can be reduced. In the following derivations, we replace the odd symmetry of the phase-difference samples given in (10) by the even symmetry of modified phase-difference samples given in (12) and (13). In so doing, we may have simplified algorithm derivations.

$$\begin{aligned} d_u(n)\cdot d_u{}^{*}(n+1) &= e^{-j\frac{\pi un(n+1)}{63}}\cdot e^{j\frac{\pi u(n+1)(n+2)}{63}} \\ &= e^{j\frac{2\pi u(n+1)}{63}} \quad ,n=0,\ldots,29 \end{aligned} \tag{12}$$

$$\begin{aligned} d_u(m+1)\cdot d_u^{*}(m) &= e^{-j\frac{\pi u(m+2)(m+3)}{63}}\cdot e^{j\frac{\pi u(m+1)(m+2)}{63}} \\ &= e^{-j\frac{2\pi u(m+2)}{63}} \quad ,m=31,32,\ldots,60 \end{aligned} \tag{13}$$

By substituting the even symmetry property of the modified phase-difference samples of (12) and (13) into (10), we have the new cost function $C_2(i,u)$, which is composed by the phase-difference correlation of the PSS.

$$\begin{aligned} &C_2(i,u) \\ &= \sum_{k=1}^{30} \left\{R_{PSS}(-k-1+i)\cdot R_{PSS}^{*}(-k+i)\right\}\cdot\left\{d_u(30-k)\cdot d_u^{*}(31-k)\right\}^{*} \\ &+ \sum_{k=1}^{30} \left\{R_{PSS}(k+1+i)\cdot R_{PSS}^{*}(k+i)\right\}\cdot\left\{d_u(k+31)\cdot d_u^{*}(k+30)\right\}^{*} \end{aligned} \tag{14}$$

Besides, notice that

$$\sum_{k=1}^{30}\left\{d_u(30-k)\cdot d_u^{*}(31-k)\right\}^{*} = \sum_{k=1}^{30}\left\{d_u(k+31)\cdot d_u^{*}(k+30)\right\}^{*} \tag{15}$$

Finally, the new cost function can be re-written by

$$\begin{aligned} &C_2(i,u) \\ &= \sum_{k=1}^{30}\left\{\left(R_{PSS}(-k-1+i)\cdot R_{PSS}^{*}(-k+i)\right)+\left(R_{PSS}(k+1+i)\cdot R_{PSS}^{*}(k+i)\right)\right\} \\ &\quad\cdot\left\{d_u(k+31)\cdot d_u^{*}(k+30)\right\}^{*} \end{aligned} \tag{16}$$

ISBN: 978-988-19252-6-8
ISSN: 2078-0958 (Print); ISSN: 2078-0966 (Online)

$$(\hat{\varepsilon}_{IFO}, \hat{u}) = \arg\max_{i,u} |C_2(i,u)| \tag{17}$$

In so doing, the requirements of the complex multipliers can be saved up to 50%.

Next, the other important issue is to investigate the characteristics of the phase-difference correlation of the PSS given in (16). Assuming that the noise is ignored, we may first rewrite (16) in the following form

$$\begin{aligned} & C_2(i,u) \\ & = \sum_{k=1}^{30} \left\{ \left(R_{PSS}(-k-1+i) \cdot R_{PSS}^*(-k+i) \right) + \left(R_{PSS}(k+1+i) \cdot R_{PSS}^*(k+i) \right) \right\} \\ & \quad \cdot \left\{ d_u(k+31) \cdot d_u^*(k+30) \right\}^* \\ & = \sum_{k=1}^{30} \left\{ \left(d_u \cdot (30-k) \cdot H(30-k) \cdot d_u^* \cdot (31-k) \cdot H^*(31-k) \right) \right. \\ & \quad \left. + \left(d_u(k+31) \cdot H(k+31) \cdot d_u^*(k+30) \cdot H^*(k+30) \right) \right\} \\ & \quad \cdot \left\{ d_u(k+31) \cdot d_u^*(k+30) \right\}^* \end{aligned} \tag{18}$$

where $H(k)$ is the frequency response on the kth subcarrier. In the light of (18), we can see that the imaginary part of the channel squared values of $H(30-k) \cdot H^*(31-k)$ and $H(k+31)H^*(k+30)$ are relatively small as composed to real part of the channel squared values. Especially, in the frequency non-selective channel, the imaginary part will be zero. For illustration, Fig. 3 shows the real part and imaginary part of the phase-difference correlation of the PSS for IFO detection. In this simulation, the IFO is with 2.0. We can obviously see that the real part values are relatively large than the imaginary part values. Thus, we can conclude that the real part values are more important than imaginary part values.

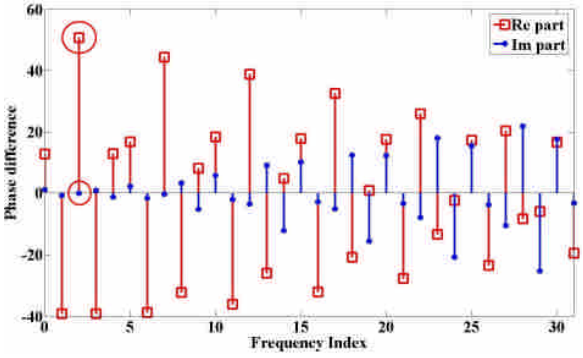

Fig. 3. Real part and imaginary part of phase-difference correlation of the PSS with IFO of 2.0

Second, we investigate the effect of the FFO on the real part and the imaginary part of the phase-difference correlation, respectively. From Fig. 4, we can obviously see that the real-part values decrease and the imaginary-part values increase as the FFO increases. Therefore, we may know that the imaginary-part values do not provide any positive information for synchronization detection algorithm given in (17) . Because of the reasons we discussed above, we finally replace the absolute operator in (17) by the real-part operator. In so doing, the detection algorithm not only can perform better, but also the computing complexity can be reduced further by saving the absolute operator circuit.

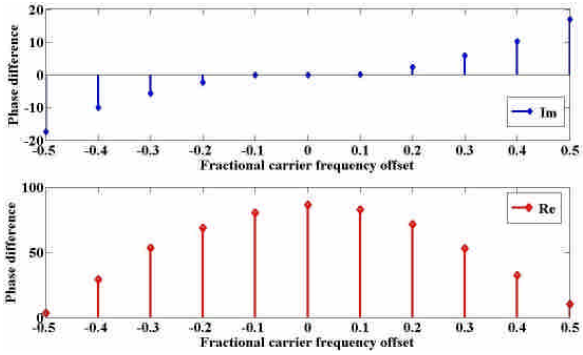

Fig. 4. Real part and imaginary part of the phase-difference correlation for different FFOs.

Finally, the improved joint detection algorithm of the IFO and sector CID is given by (19).

$$(\hat{\varepsilon}_{IFO}, \hat{u}) = \arg\max_{i,u} \quad \mathrm{Re}(C_2(i,u)) \tag{19}$$

V. Simulation Results

The simulation parameters for the LTE Downlink are listed in TABLE II [1].

TABLE II.
Simulation Parameters for the LTE Downlink

Parameters	Value
Frame structure	FDD
Bandwidth	5MHz
CP type	Normal CP
Symbol alphabet	QPSK
Channel model	time-dispersive channel
Number of users	1
CP detection	Perfect
Doppler rate	0 Hz

In the following simulations, we use two channel power delay profiles. First, the channel power delay profile is modeled as six-ray power-delay profile with equal-gain power, as depicted in Fig. 5.

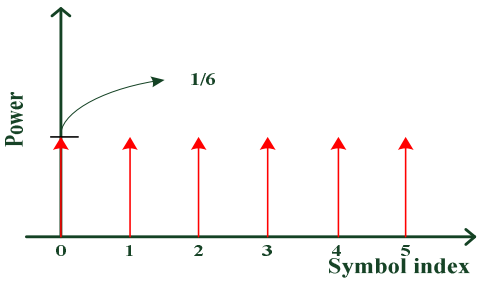

Fig. 5. The six-ray power-delay profile

Second, the channel power delay profile is exponentially decayed. The channel model is expressed by

$$h(t) = \sum_{p=0}^{P-1} \alpha_p \delta(t - \tau_p) \tag{20}$$

where P is the number of multipath, τ_p is the pth-path delay time, α_p is the pth-path complex gain. Each path gain is a complex random variable with uniformly distributed phases and Rayleigh distributed magnitude. The average power of each path decays exponentially.

ISBN: 978-988-19252-6-8
ISSN: 2078-0958 (Print); ISSN: 2078-0966 (Online)

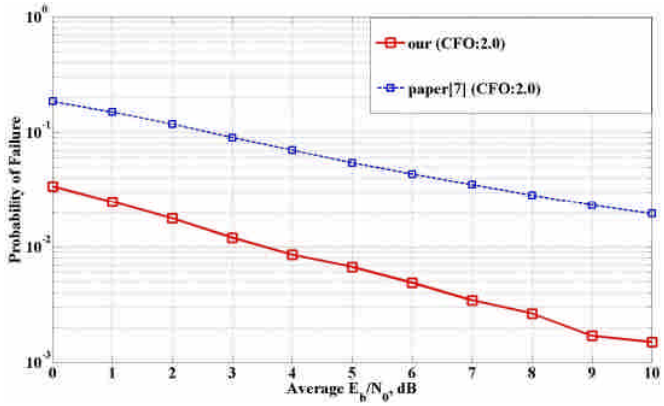

Fig. 6. Error Probability of IFO estimation without FFO compensation in 6-ray equal-gain power-delay profile channel.

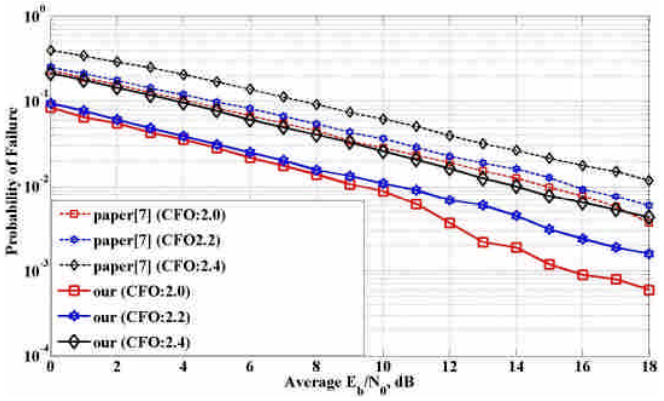

Fig. 7. Error Probability of IFO estimation without FFO compensation in exponentially decayed power-delay profile channel.

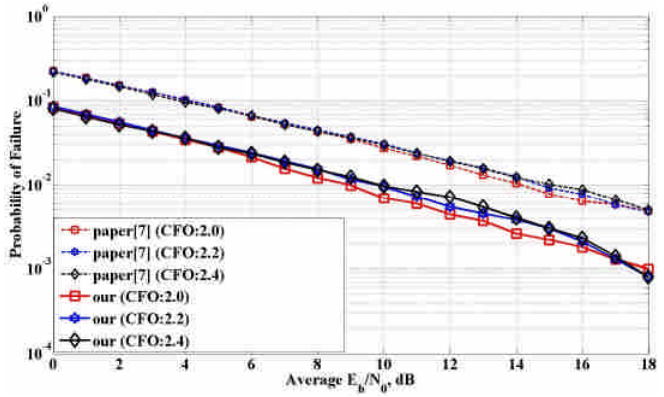

Fig. 8. Error Probability of IFO estimation with FFO compensation in exponentially decayed power-delay profile channel.

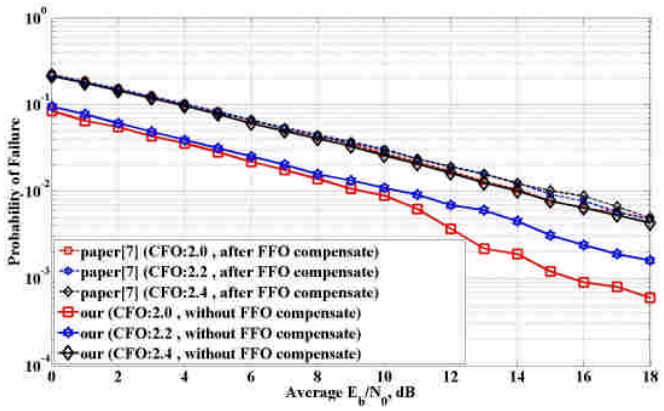

Fig. 9. Error Probability of IFO estimation in exponentially decayed power-delay profile channel.

From Fig.6 to Fig.8, we can obviously see that the proposed detection algorithm is always better than that of the method in [7], no matter the FFO is compensated or not. Moreover, from Fig. 9, it is also illustrated that our method in the case of large FFO is also robust than that of [7] in the case of the small FFO. This is because that in the case of large FFO, the imaginary part of the wrong IFO will be enlarged and correspondingly causes the algorithm (11) even worse. But our method given in (19) only takes the real part of the phase-difference correlation, and thus can reduce the error in estimating IFO. Next, in the light of result of the Fig. 4, the real part of the phase-difference correlation remains relatively high only when the FFO is in the range of (-0.2, 0.2). Therefore, we suggest that when the FFO is beyond the range of (-0.2, 0.2) the FFO should be first compensating before estimating the IFO.

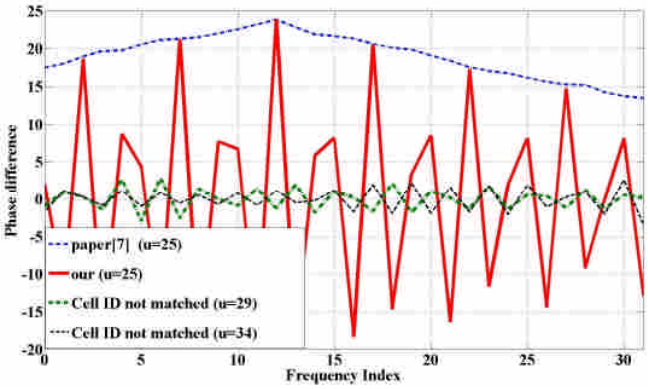

Fig. 10. Joint detection waveforms of IFO and sector CID in in exponentially decayed power-delay profile channel.

In the Fig. 10, we assume that the FFO is perfectly compensated and let the IFO be 12 and root index u=25. Therefore, the maximum value of the proposed detection algorithm shown in Fig. 10 only occurs in the IFO of 12 and u=25. From Fig. 10, we can see that our proposed method can effectively suppress the wrong IFOs especially which are neighbors of the correct IFO. Because of this reason, we can then reduce the error rate of the joint detection of IFO and sector CID. Besides, as given in equation (16), our proposed detection algorithm use the symmetry property of the PSS to save 30×3=90 complex multipliers or equivalently save the requirement of multipliers up to 50 %.

VI. Conclusion

In this paper, we use the symmetry property of phase-difference samples between the PSS to reduce the computing complexity of the proposed joint detection algorithm of the IFO and sector CID. First, because the first 30 difference samples and last 30 difference samples are even symmetry, the joint detection algorithm can save half of requirements of the multipliers as compared to that required in [7]. Equivalently, the detection algorithm can save 90 complex multipliers. Besides, we analyze the characteristics of the phase-difference correlation of the PSS, and find that its real part values decrease as the FFO increases, but its imaginary part values increase as the FFO increases. Thus, we modify the synchronization detection algorithm where we replace absolute operator [7] by real-part operator. Besides, after compensating the FFO, the algorithm is more dominant

ISBN: 978-988-19252-6-8
ISSN: 2078-0958 (Print); ISSN: 2078-0966 (Online)

by the real-part values of the phase-difference correlation. This is why our proposed algorithm is robust than the algorithm presented in [7]. Moreover, our proposed algorithm can still maintain acceptable detection performance in the case of the small FFO if not compensating the FFO previously. To sum up, our proposed joint detection algorithm of IFO and sector CID can serve as a low complexity and high performance candidate for downlink LTE synchronization.

ACKNOWLEDGMENT

This research work is supported by College of Electrical Engineering and Computer Science, Chung Yuan Christian University, under the Grant no. CYCU-EECS-10002.

REFERENCES

[1] 3GPP TS 36.211 v10.3.0, "Physical channel and modulation," Sept.2011.

[2] J. J. van de Beek, M. Sandell, and P. O. Borjesson, "ML estimation of time and frequency offset in OFDM system," *IEEE Transactions on Signal Processing*, vol. 45, pp. 1800–1805, Jul. 1997.

[3] D. Toumpakaris, J. Lee, and H. Lou, "Estimation of integer carrier frequency offset in OFDM systems based on the maximum likelihood principle," *IEEE Transactions on Broadcasting,* vol. 55, pp. 95–108, March 2009.

[4] M. Morelli, A. N. D'Andrea, and U. Mengali, "Frequency ambiguity resolution in OFDM systems," *IEEE Commun. Lett.,* vol. 4, pp.134–136, Apr. 2000.

[5] T. M. Schmidl and D. C. Cox, "Robust frequency and timing synchronization for OFDM", *IEEE Trans. Commun*., vol.45, pp.1613-1621, Dec. 1997.

[6] K. Manolakis, D. M. Gutierrez Estevez, V. Jungnickel, W. Xu and C. Drewes, "A closed concept for synchronization and cell search in 3GPP LTE systems, "*IEEE Wireless Communications and Networking Conference (WCNC) , pp.1-6,Apr.2009.*

[7] Pei-Yun Tsai and Hsiang-Wei Chang, "A New Cell Search Scheme in 3GPP Long Term Evolution Downlink OFDMA Systems". *IEEE WCSP*, 2009.

ISBN: 978-988-19252-6-8
ISSN: 2078-0958 (Print); ISSN: 2078-0966 (Online)